Available online at www.sciencedirect.com

ScienceDirect

Ceramics International 40 (2014) 3011–3021

CERAMICS INTERNATIONAL

www.elsevier.com/locate/ceramint

Diffusion bonding of alumina using interlayer of mixed hydride nano powders

Navid Hosseinabadi[a], Rasoul Sarraf-Mamoory[a,*], Ali Mohammad Hadian[b]

[a]*Materials Engineering Department, Tarbiat Modares University, P.O. Box 14115-143, Tehran, Iran*
[b]*School of Metallurgy, Tehran University, P.O. Box 162352-1254, Tehran, Iran*

Received 20 August 2013; accepted 4 October 2013
Available online 15 October 2013

Abstract

In this study, mixed hydride/alanate nano powders in the Al–Mg system were used as the interlayer for low temperature diffusion bonding of dense alumina parts. Decomposition of hydride nanopowders at bonding temperatures in-situ formed metals and alloys nano particles with oxide free surfaces and high sinter-ability in the interlayer. Nano powders sintering behavior in the interlayer and formation of compounds in the reaction layer during diffusion bonding were studied. Mixture of 50–50 M ratio of AlH_3 and $Mg(AlH_4)_2$, as the interlayer improved bond strength of the joints. Diffusion bonding products were formed in the $MgO–Al_2O_3$ spinel system with different stoichiometries. Bond strength improved up to 202 MPa by induction hot pressing alumina parts at low bonding temperature of 400 °C under pressure of 20 MPa during 30 min bonding period.

Keywords: D. Al_2O_3; Diffusion bonding; Hydride; Alanate; Nanopowder

Introduction

Oxide based ceramic bodies, with exceptional physical and mechanical properties at corrosive and high temperature mediums and high wear resistance with low friction coefficients, have been used in many different industries as semiconductors, insulators, and armors [1,2]. Despite the unique properties of the engineering oxide ceramics in optical, electronic, refractory, and tribological fields, many applications require special shapes in each dimension which can be achieved by using different parts with reliable joints. These bonding processes required the developments in techniques to join ceramics to ceramics/metals [2]. Ceramic parts can be bonded via various methods: (i) transient liquid interlayer bonding, (ii) refractory braze alloys, (iii) refractory glass bonding, (iv) bonding using polymer precursors, and (v) diffusion bonding. Among these techniques, brazing and diffusion bonding are more suitable methods and had been the subject of many researches [3–5]. Diffusion bonding is mostly carried out by holding two nominally flat surfaces together at elevated temperatures. Bonding happens in three steps: (i) elimination of interfacial voids by material transition or compaction, (ii) adhesion by atom flow relaxation or grain formation, and (iii) chemical reaction and phase formation along interfaces [6]. Direct diffusion bonding of oxide ceramic parts requires high pressures and temperatures, up to 250 MPa and 1500 °C, resulting exaggerated grain growth in parts [7]. Mutual bonds form via diffusion along interfaces, diffusion in outer layers of bulk (for ceramics and metals) or plastic flow after yield and creep (for metals). As seen, based on presence of metal interlayers (as foils or powders) combination of controlling mechanisms can be activated which can moderate pressure and temperature of the process [8]. Hybrid diffusion bonding processes like transient liquid phase bonding (TLPB) and partially transient liquid phase (PTLPB) are based on melting or partially melting metal interlayers during heating, liquid flow and filling voids, and resolidification [7,9]. Residual metallic interlayer materials affect joint strength and operating temperature range of bonded parts [9]. Most diffusion bonded parts (like laminate composites) with dense bulk or foil interlayers showed defects like un-joined areas, cracked ceramic surfaces, inclusions

---

[*] Corresponding author. Tel./fax: +98 21 82883308.
E-mail address: rsarrafm@modares.ac.ir (R. Sarraf-Mamoory).

0272-8842/$ - see front matter © 2013 Elsevier Ltd and Techna Group S.r.l. All rights reserved.
http://dx.doi.org/10.1016/j.ceramint.2013.10.006

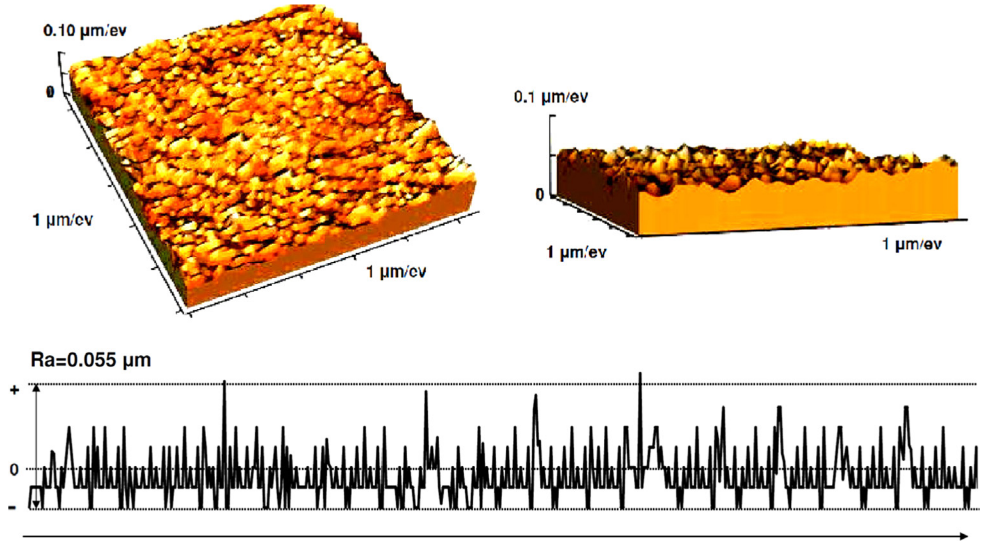

Fig. 1. Surface roughness of the alumina parts before diffusion bonding with 150 μm linear profile.

along interlayers, and pores near joint surfaces [8,10]. Using mixtures of powders as the interlayer materials improved bond qualities along mutual surfaces by activation of rapid sintering of powders during joining processes [11]. High activity and sinterability of nano-sized powders in interlayers improved bonding qualities [12]. Sintering process in interlayers can coincide with reactions between interlayer materials and oxide ceramic surfaces, like formation of mixed ceramics (RR'_2O_3) in oxide systems [10,13]. In-situ formed nano powders with minimum surface contaminations like surface oxides can improve diffusion bonding processes by reducing bonding pressure and temperature during sinter–welding process [14–16].

In this study, mixed metallic hydride and alanate nanopowders were used as the interlayer materials for diffusion bonding of alumina parts using the induction hot pressing system. Effects of interlayer on bond formation at lower temperature and pressures, inter layer powders sinter-ability (axial shrinkage), and bond properties like shear strength were studied.

1. Materials and methods

Solid state diffusion bonding of ceramic bodies was carried out by applying sufficient pressure on ceramic bodies with appropriate interlayer in temperatures lower than the melting point of the parts, especially interlayer nanopowders. Powders of polycrystalline alumina ((Al_2O_3, $>95\%$ pure (<1 wt% CaO, <0.5 wt% MgO, <1 wt% Fe_2O_3, <1 wt% Cr_2O_3, <1 wt% TiO_2)), Grauf Klaus Gmb, Germany) were used to manufacture disks with ϕ17 mm and 5 mm height. Pressureless sintering regime of uni-axial pressing at 100 MPa with 1650 °C sintering temperature for 24 h dwelling time and 36 h cooling under air atmosphere was applied for manufacturing ceramic bodies. The surfaces of Al_2O_3 bodies to be joined were ground using 400, 600, 1000, and 1200 grid silicon carbide papers, followed by polishing with diamond paste and Al_2O_3 suspension to achieve average surface roughness of Ra: ~55 nm, measured by non-contact mode atomic force microscopy (AFM, solver P47H instrument). Roughness profile was analyzed along surfaces. A schematic micrograph of polished surface roughness and roughness profile are shown in Fig. 1. Alumina bodies were cleansed before bonding using a three stage washing process, consisting of 30 min in de-ionized water medium with supersonic wave to remove residual debris, 30 min in methanol medium for degreasing, and 30 min in acetone medium for final wash and dehumidifying. The interlayers, AlH_3 and $Mg(AlH_4)_2$ nanopowders, were synthesized via mechano–chemical activation process (MCAP). The interlayer was applied using custom designed Cr-steel die and blade tape casting instrument. The thickness of the interlayer could be controlled with 10 μm precision by turning treaded spindle. A schematic image of the mechanism is shown in Fig. 2. Nitromethane (CH_3NO_2), a non-reactive liquid with hydride/alanate, was used to make starting 90 wt% nano powder mixtures (pastes) for tape casting. 50 μm thickness interlayers

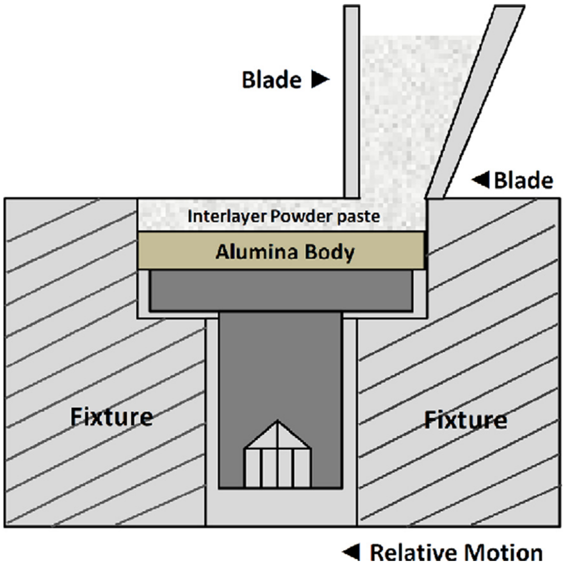

Fig. 2. Schematic view of custom designed tape casting die and blade.

were chosen to study the diffusion bonding procedure. The diffusion bonding samples were two Al_2O_3 disks mounted axially with hydride/alanate nanopowder pastes in the middle. The samples were kept for 1 hour in a custom made glove box under 10^{-4} MPa vacuum and high purity dry argon gas in room temperature to avoid any air/moisture exposures and complete extraction of nitromethane from the pastes. Samples were placed carefully in a two-punch cylindrical graphite die. The die assembly was setup in a custom made uni-axial hot press. Schematic representation of the induction hot press mechanism and die assembly is shown in Fig. 3-a. The induction hot press heating system supplied heating rates up to 300 °C/min, with maximum operating temperature of 1500 °C in dies. Thermal sensor was placed at a hole in the die near the sample to achieve accurate temperature. A two cylinder (up and down) hydraulic pressing system could obtain loads up to 20'000 N force. The induction hot press chamber was evacuated and the pressure of $\sim 10^{-4}$ MPa was maintained during the tests. Different hot pressing temperatures, with constant pressure and dwelling time were examined. The bonding procedure was as follows: cold pressing up to the assigned pressure, heating up to the temperature (100 °C/min), holding for the assigned dwelling time, and fast cooling (250 °C/min) to room temperature. Axial shrinkage normal to the bonding assembly was studied by recording punches displacements during bonding process (zeroed at initial shrinkage after cold pressure) using position sensors with 10^{-4} mm accuracy. The bond strength was measured using custom designed Cr-Steel 4 pin fixture for holding the samples and semi circular jig holder attached to the universal testing machine (Instron No. 5565; InstronCorp, Canton, Mass) and the load was applied by jig with diameter of 19 mm corresponding to the diameter of the ceramic bodies. A load was applied at the speed of 0.50 mm/min until failure of the bond. Average bond strengths (MPa) were calculated by dividing the load (N) at which failure occurred by the nominal bonding area (mm^2). Schematic view of the shear strength test assembly is shown in Fig. 3-b. The phase structure of samples was checked by XRD analysis of exposed surfaces using Philips MPD-XPERT mono chromatic $Cu_{k\alpha} = 0.154$ nm at voltage of 46 kv and 8 mA current. The scan range was between $2\theta = 10°$ and 90° and the scan rate was 1° per min at the step size of 0.02°. Diffraction angles were reported based on best fitting range. Nano grain/crystallite sizes were calculated based on peak broadening using Cauchy/Gaussian approximation by linear regression plot by equation [4]:

$$\frac{\delta^2(2\theta)}{\tan^2(\theta)} = \frac{K\lambda}{D}\left[\frac{\delta(2\theta)}{\tan(\theta)\sin(\theta)}\right] + 16\varepsilon^2 \quad \text{and} \quad \delta(2\theta) = B\left[1-\left(\frac{b^2}{B^2}\right)\right]$$

The term δ (2θ) indicates instrumental-broadening correction where $K\lambda/D$ is the slope and D is the mean crystallite (nano grain) size. K is a constant about 1 and ε indicates the accumulated strain in the structure. Term θ is the position of the analyzed peak. B and b are the breadth of same peak (the full widths at half maximum, FWHM) of experimental and reference crystal, both in radians, respectively. Lattice parameters of phases were calculated using d spacing from Bragg equation and related lattice equations.

Differential scanning calorimetry (DSC) was performed using Netzsch404 instrument. About 15 mg of samples were heated in an alumina crucible at the scan rate of 2, 5, and10 °C/min under high purity Ar flow for indication of reaction (dissociation) temperatures of samples. Thermo-gravimetric analysis (TGA) was performed using STA 1460 equipment instrument with 15 mg samples heated at a heating rate of 10 °C/min, under nitrogen flow for measuring the amount of hydrogen release in samples during heating cycle, as an acceptable estimation for constrained hydride mixture in bonding assembly.

Morphology of nanopowders and surfaces was observed using scanning electron microscopy (SEM-Philips, XL30 series) with an accelerating voltage of 10.0–15.0 kV, FE-SEM (Hitachi, 501 xr) at accelerating voltage of 15.0–17.0 kV, and transmitting electron microscopy (TEM-Hitachi 2100) with an accelerating voltage of 50.0 kV.

2. Results and discussion

The mechanical and physical properties of the sintered bodies were measured as MOR: 590–620 MPa (four point bending, $20 \times 40 \times 80$ cm^3 samples), hardness: $\sim$2150 vickers (9.81 N), and density: $\sim$3.9 g/cm^3 for five samples with smooth faces and edges. Aluminum hydride (AlH_3), magnesium alanate($Mg(AlH_4)_2$), and mixtures of both were used as the hydride interlayer mixtures.

The XRD patterns of the hydride nanopowders are shown in Fig. 4. As seen, the patterns contain characteristic peaks of pure AlH_3 and $Mg(AlH_4)_2$. Alane phase was crystallized in centered rhombohedral crystal structure and $Mg(AlH_4)_2$ was formed in terigonal (HCP) crystal structure. Detailed information of crystal structures is reported in Table 1.

AlH_3 and alanates are mostly unstable (thermodynamically) in a large temperature range but their decomposition is kinetically limited [17]. DSC results were used to study the thermal behavior of the hydrogen release like dissociation temperature, steps, and the activation energy of hydride/alanate decomposition. DSC and DTA patterns of AlH_3 and $Mg(AlH_4)_2$ are shown in Fig. 5. With constant increase of temperature, hydrides/alanates decompositions happen with thermal energy absorption/desorption (endothermic/exothermic).The DSC patterns contains a one step dissociation of AlH_3 near 150 °C with an endothermic peak, and two steps dissociation of $Mg(AlH_4)_2$ with an exothermic peak at 130 °C and an endothermic peak about 285 °C. The exo/endothermic behavior of mixture indicates the energy necessary during bonding process for hydride mixture dissociations and was used by the hot press induction system. The amount of hydrogen release at each step of dissociation and the main dissociation reaction at each step in a close weight change range of 100% to 90% are also shown in Fig. 5. AlH_3 showed one step weight loss (hydrogen dissociation) up to $\sim$8 wt% near 150 °C which is smaller than theoretical amount of $\sim$10 [18]. $Mg(AlH_4)_2$ clearly showed the two step dissociation behavior with total hydrogen content of $\sim$9.2 wt%.

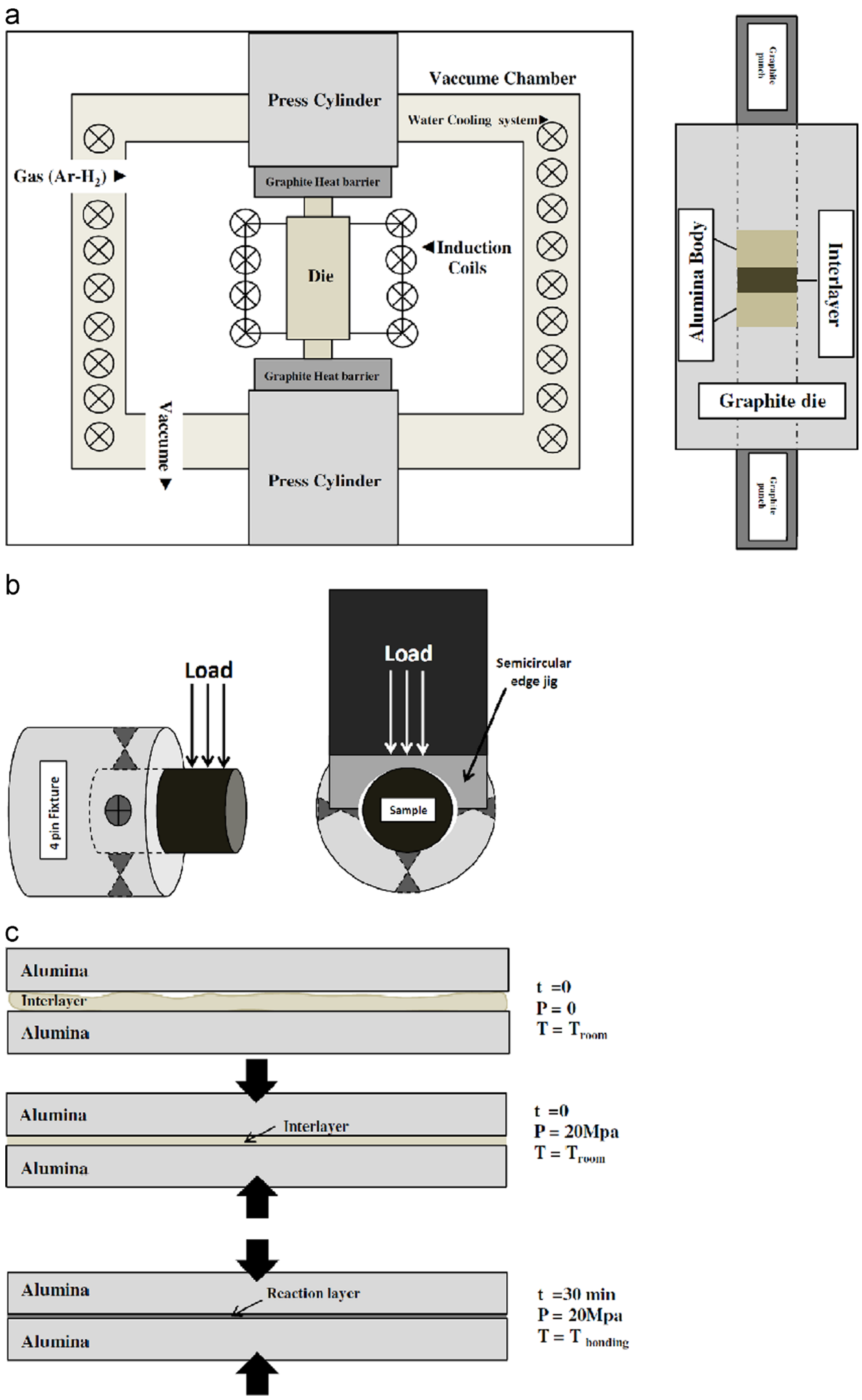

Fig. 3. (a) Schematic representation of the hot press mechanism and die assembly, (b) schematic view of the shear strength test assembly, and (c) schematic view of the diffusion bonding process with nano-sized hydride interlayers.

The products of hydride dissociation are combinations of metals and alloys, a suitable delivery system for pure/alloyed nano-sized metal particles. In-situ formation of metals and alloys via dissociation of hydride mixtures is a key part of this study. The residual materials of DSC analysis were analyzed by XRD. The patterns are shown in Fig. 6. No characteristic peaks for Al, Mg, or their complex oxides were detected. By increasing temperature during bonding process, the hydride

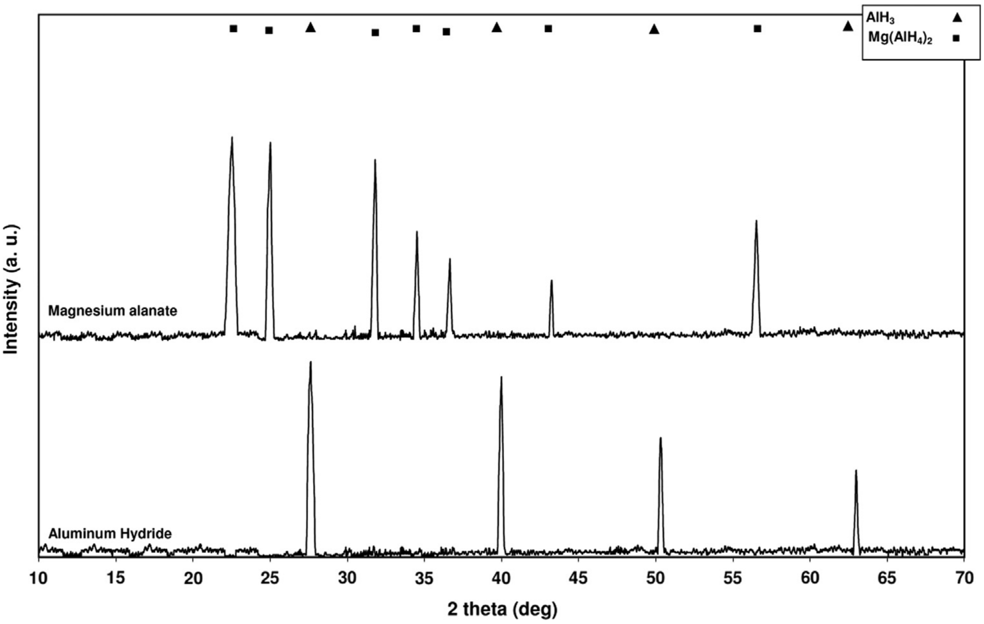

Fig. 4. XRD patterns of the hydride nanopowders.

Table 1
Crystal system, lattice parameters, lattice volume, lattice volume change percent, and calculated crystallite size of alane, magnesium alanate, aluminum, and magnesium alloy.

Hydride	Crystal structure	Lattice parameters (Å) ±0.001	$\Delta a/a_0$ (%) $\Delta c/c_0$ (%)*	Lattice volume (Å^3) ±0.0001	$\Delta v/v_0$ (%)*	Crystallite size (nm)
AlH$_3$	Rhombohedral	a=b=4.450 c=11.805	0.02 0.02	202.4435	0.06	10
Mg (AlH$_4$)$_2$	Trigonal	a=b=5.199 c=5.858	0.00 0.00	137.1219	0.00	9
Al	FCC	a=4.08	0.77	67.92	0.02	9
Mg	HCP	a=3.119 c=5.209	−2.80 −0.04	43.88	−0.05	12

*regarding to standard pattern lattice parameters.

interlayer mixtures will decompose to mixtures of residual metals. Pure metallic Al and Mg–Al were the products of heating AlH$_3$ and alanate, respectively. Alloying with Al moved the Mg (HCP) characteristic peaks up to higher degrees while interstitial solution of Mg in Al guides its characteristic peaks to lower angles. Detailed properties of remaining metals and alloys are mentioned in Table 1. Interstitial entrance of Al into Mg structure caused the unit cell contraction in Mg alloyed phase.

Interlayers of AlH$_3$ (A), Mg(AlH$_4$)$_2$ (M), and 1–1 M ratio mixed powder (AM) were studied for diffusion bonding Al$_2$O$_3$ bodies in three different temperatures. Table 2 summarizes diffusion bonding (hot pressing) conditions and results for different bonding assemblies. Visual inspection of samples showed no surface cracks, ceramic bodies rupture, or joining to the graphite die surfaces. As seen, low temperature–pressure diffusion bonding was achieved in different conditions and only the A-200 sample cleaved to two separated bodies during extraction from graphite die. Diffusion bonding of Al$_2$O$_3$ bodies with nano-sized hydride interlayers consists of three stages: (i) Compaction of the hydride nanopowders during cold pressing by 20 MPa pressure which helps uniform distribution of interlayers along alumina bodies surfaces and filling empty gaps and voids between agglomerates with ~40 μm compaction in all samples, (ii) heating up to the bonding temperature which caused decomposition of hydride interlayer to metals, alloys, and intermetallics, and (iii) keeping at bonding temperature under pressure which leads to sintering and reaction bonding along the bonding surfaces. Schematic view of the process is shown in Fig. 3-c. By proceeding diffusion bonding (hot pressing) and sintering processes, the interlayer mixture transforms to the narrower sintered reaction layer which can be detected via axial shrinkage parallel to the direction of applied pressure. The shrinkage behavior of the samples versus bonding time after applying bonding pressure (20 MPa) and heating up to the bonding temperature is shown in Fig. 7. Small fluctuations in patterns were caused by vibrations of the hot press hydraulic pressure system. Hydride decompositions happened at the early stages of heating and the rest of the bonding process was enhanced by forming reaction layers and nanopowders sintering. Samples had different shrinkage behavior in slope and the straight parts of the patterns. As expected,

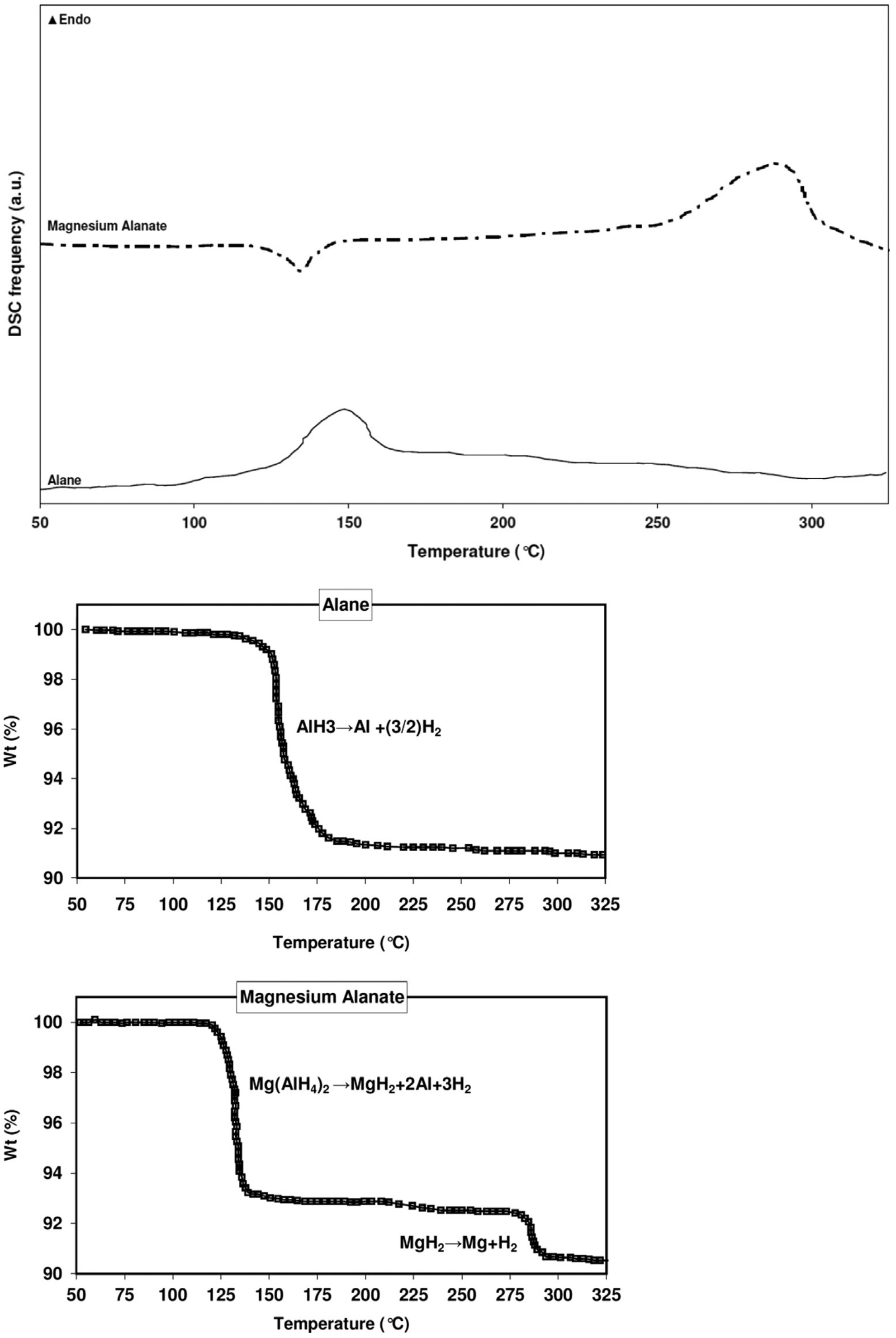

Fig. 5. DSC and DTA patterns of alane and magnesium alanate.

the axial shrinkage increased at higher bonding temperatures, caused by proceeding of sintering process. AlH_3 interlayer samples (A) had the lowest amount of shrinkage regarding to alanate (M) and mixed samples (AM). The net amount of shrinkage in A samples were 2, 2.5, and 5 μm in 200, 300, and 400 °C, respectively. By increasing bonding temperature, maximum shrinkage happened earlier and moved from near 25th minute to near 20th minute of the diffusion bonding process. A-300 sample showed a more abrupt increase while A-200 and A-400 had gradual increase in shrinkage which indicates activation of a sintering/reactive process at temperatures near 300 °C. Same process had caused fast sintering in the early stages of A-400 sample. The amount of axial shrinkage increased in M samples at all temperatures, comparing to A samples. Samples showed gradual increase during bonding without any sudden change. Axial shrinkage was

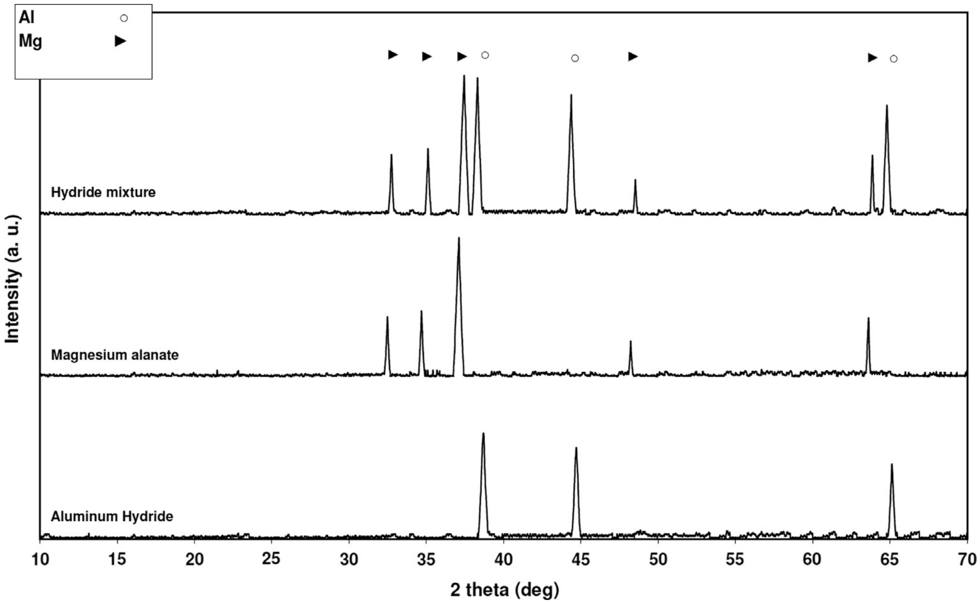

Fig. 6. XRD patterns of the heated hydride nanopowders.

Table 2
Joining results in different diffusion bonding conditions.

Sample	Pressure (MPa)	Temperature (°C)	Duration (min)	Atmosphere	Bond result[a]
A-200	20	200	30	vacuum	✗
A-300	20	300	30	vacuum	✓
A-400	20	400	30	vacuum	✓
M-200	20	200	30	vacuum	✓
M-300	20	300	30	vacuum	✓
M-400	20	400	30	vacuum	✓
AM-200	20	200	30	vacuum	✓
AM-300	20	300	30	vacuum	✓
AM-400	20	400	30	vacuum	✓

[a] Bonded (✓) and unbonded (✗)

measured as 3, 4, and 6 for M-200–M-400, respectively. Maximum shrinkage happened earlier than A samples and was constant for near half of the diffusion bonding period. Same behavior was detected in mixed samples (AM) with shrinkages of 5, 6, and 7.6 μm in AM-200–AM-400 samples, respectively.

The strength of the diffusion bonded alumina bodies is affected by the products of reactions along ceramic–interlayer surfaces and extent of the sintering process in interlayer mixtures. In order to evaluate the quality of diffusion bonding, shear strength of the samples was measured, based on the shear load necessary to separate ceramic bodies along nominal contact surface areas. The shear strength stress versus displacement along bonding surface of different diffusion bonded samples is shown in Fig. 8. The patterns are consisted of one out of three for each sample which represents samples behavior under shear load. All samples separated along the bonding surface without any defect to Al_2O_3 bodies. A-200 sample, despite experiencing some axial shrinkage, showed no shear strength under load. Patterns have a similar shape with rapid ascending to the maximum and sudden descending after maximum without plastic deformation along the reaction layer. Separation of all samples happened with small deflections less than 0.1 mm. No sign of deformation or shear was detected in alumina bodies. Increasing bonding temperature in all samples (A, M, and AM) improved the bond shear strength. Maximum strength by increasing bonding temperature were 135 and 136 MPa in A samples, 147, 155, and 190 MPa in M samples, and 171, 175, and 202 MPa in AM samples. Presence of magnesium increased the strengths in M samples, while mixing with additional AlH_3 further improved the shear strength up to 9% in AM samples. This fact can indicate the role of magnesium in enhancing sintering processes and formation of stronger reactive products with Al_2O_3 surfaces. XRD analysis of the samples was carried out on the surfaces after shear strength test to indicate reaction products along joined surfaces. The nature of the reaction layer products indicates the bond strength and quality. Fig. 9 shows XRD patterns for all samples. Strong characteristic peaks of the Al_2O_3 were detected in all samples which are mostly related to X-ray penetration to the base alumina bodies. Two different classes of reactions happened during diffusion bonding: (i) decomposition of metal hydride and alanate and their mixtures,

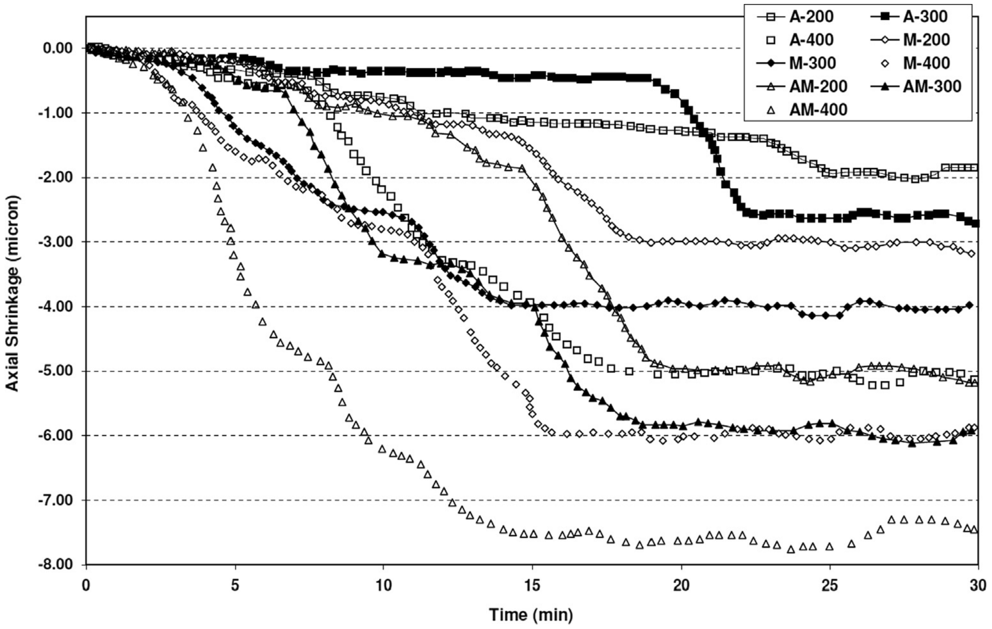

Fig. 7. The shrinkage behavior of the samples versus bonding time.

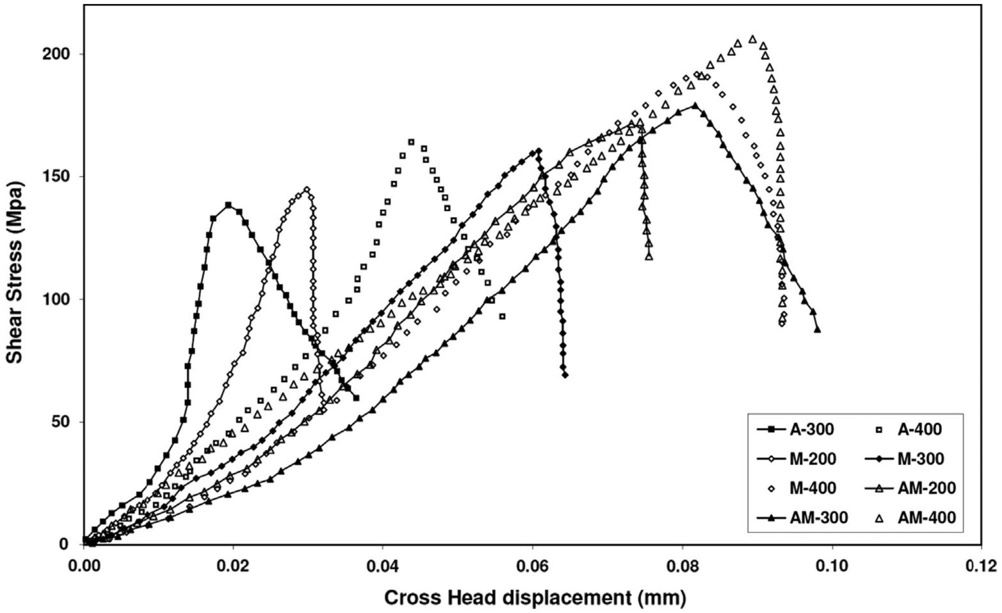

Fig. 8. The shear strength curves of the different diffusion bonded samples.

as follows:

$$AlH_3 \rightarrow Al + (3/2)H_2$$

$$M_g(AlH_4)_2 \rightarrow M_gH_2 + 2Al + 3H_2$$

and

$$MgH_2 \rightarrow Mg + H_2$$

(ii) reactions between residual metals/alloys along ceramic surfaces. Strong joints require diffusion of elemental atoms to ceramic bodies and mutual bonds formations. Main reactions which can control reactive bonds are based on oxide formations by elemental atoms, oxygen in alumina structure or residual oxygen in medium or due to decomposition by atomic hydrogen. Schematic (non-stoichiometric) reactions during heating can be like [19,20]:

$$\langle Al\rangle + \langle Mg\rangle + Alumina \rightarrow Al + Mg + [Al]_{alumina} + [Mg]_{alumina} :$$

solution of metal atoms in oxide interfaces;

$$\langle Al\rangle + \langle Mg\rangle + Alumina \rightarrow [AlO]_{Al/Mg} + [O]_{Al/Mg} :$$

solution of oxide/oxygen in metal particles;

$$\langle Mg\rangle + Alumina \rightarrow [Al]_{MgO} + [O]_{MgO} :$$

dissociation of oxide and formation of new oxides

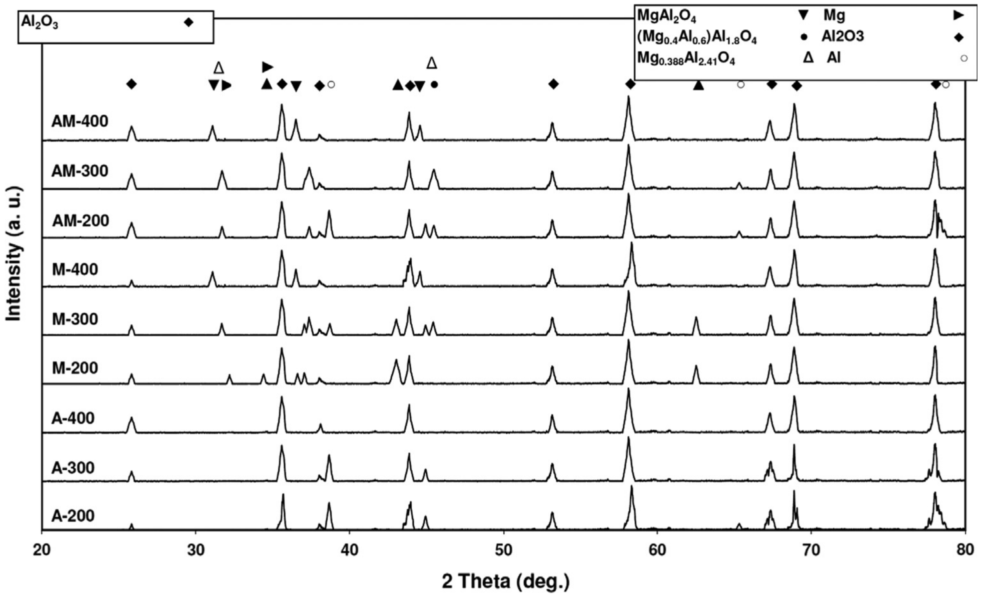

Fig. 9. XRD patterns of the reaction layer of diffusion bonded samples.

Table 3
Crystal system, lattice parameters, lattice volume, lattice volume change percent, and calculated crystallite size of reaction layer products.

Sample	Phase	Crystal structure	Lattice parameters (Å) ±0.001	$\Delta\alpha/\alpha_0$ (%)	Lattice volume (Å^3) ±0.0001	$\Delta v/v_0$ (%)*	Crystallite size (nm)
AM-400	$MgAl_2O_4$	FCC	$a=8.11$	−0.18	533.4117	−0.553	51
AM-300	$(Mg_{0.4}Al_{0.6})Al_{1.8}O_4$	FCC	$a=7.964$	−0.11	505.1191	−0.338	42
AM-200	$(Mg_{0.4}Al_{0.6})Al_{1.8}O_4$	FCC	$a=7.89$	−1.04	491.1691	−3.091	36
M-400	$Mg_{0.388}Al_{2.41}O_4$	FCC	$a=8.118$	−0.09	534.9918	−0.258	63
M-300	$MgAl_2O_4$	FCC	$a=7.96$	−0.23	504.3583	−0.675	47

*Regarding to standard pattern lattice parameters

$$\langle Mg\rangle + Al_2O_3 \rightarrow \langle MgAl_2O_4\rangle + O\uparrow :$$

Formation of inermetallic and evolution of O;

$$\langle Al(Mg)\rangle + O/Al_2O_3 \rightarrow \langle Al_2O_3\rangle + \langle MgAl_2O_4\rangle$$

and

$$\langle Mg(Al)\rangle + O/Al_2O_3 \rightarrow \langle MgAl_2O_4\rangle :$$

reaction with medium to form an oxide/intermetallic mixed oxide.

Solution of metals in oxide interfaces and oxygen/oxides/intermetallics in metal/alloy particles during heating causes super saturation during cooling and precipitation of oxides/intermetallics along the interfaces and formation of the reaction layer. Samples showed combinations of reaction products in different bonding temperatures and interlayers. In A-200 sample, characteristic peaks of non-reactive Al were detected which could be caused by low temperature of bonding, leaving some free metallic Al in the interlayer. Increasing bonding temperatures to 300 and 400 °C caused continuous decreases in Al peak intensities. A-400 sample showed no Al peaks which with improved shear strength of the sample can indicate participation of free Al atoms in Al_2O_3 phase structure formation along bonding surface. Free magnesium atoms formed by decomposition of $Mg(AlH_4)_2$ in M samples formed different phase structures in different temperatures. As seen, no sign of reaction between Mg and Al_2O_3 was detected in M-200 sample. The sample was consisted of free (non-reactive) magnesium with magnesium oxide (MgO) phase. Increasing bonding temperature to 300 °C caused more participation of Mg in oxide formation while the competition between Al and Mg caused residual Al in the reaction and formation of non-stoichiometric mixed oxide. Formation of $Mg_{0.388}Al_{2.41}O_4$ coincided with formation of MgO in the reaction layer. Increasing bonding temperatures led to participation of residual Al and MgO in formation of stoichiometric mixed oxide with spinel crystal structure ($MgAl_2O_4$). Presence of mixed oxides happened in lower temperatures in AM samples with different stoichiometry of $(Mg_{0.4}Al_{0.6})Al_{1.8}O_4$. Residual metals were seen only as atomic Al in AM-200 sample. Final reaction products in AM-400 sample were detected by sharp and relatively broad peaks of Al–Mg spinel. Comparing formed phases in the samples with alumina–magnesia equilibrium phase diagram [21] shows that the most of these non-stoichiometric phases are not stable in equilibrium conditions. Spinel can be formed in 70 wt% mixture of alumina with magnesia and mostly exist as a mixture with corundum or periclase. Non-equilibrium conditions of the process and active nature of in situ formed metals and alloys led to the formation of non-stoichiometric phases with spinel based structure.

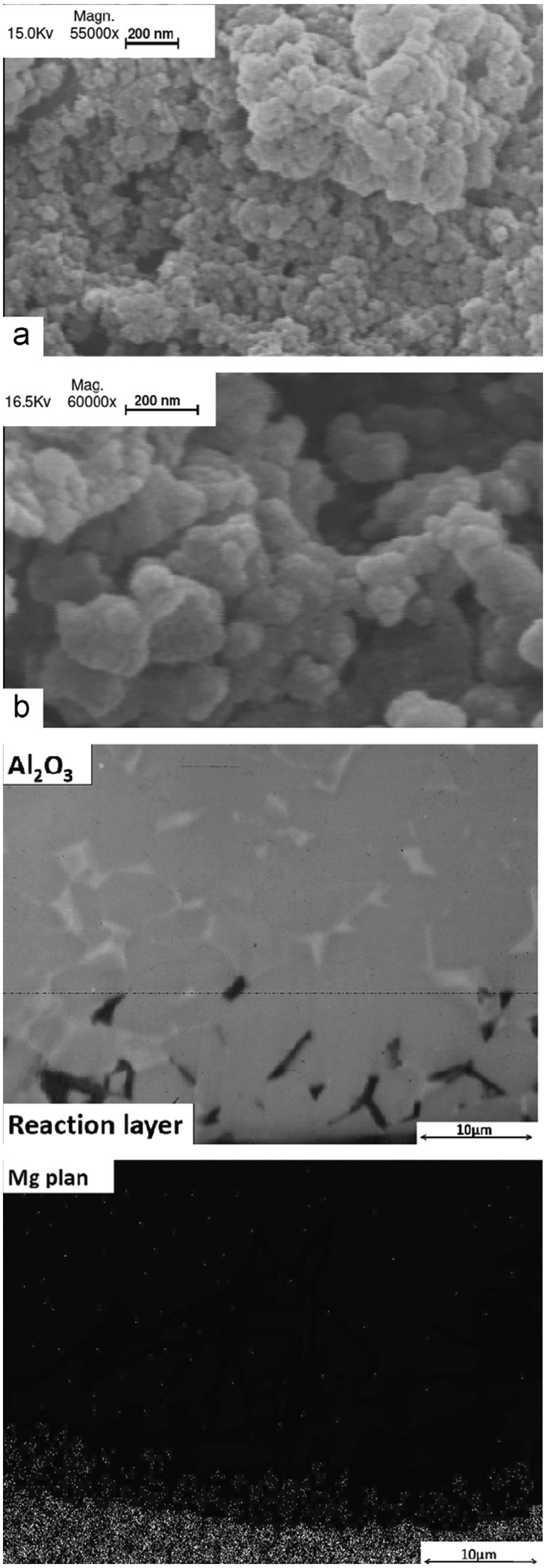

Fig. 10. FE-SEM micrographs of mixed hydride (AM) naopowers: (a) as made, (b) after heating process and SEM micrograph and magnesium map of the AM-400 sample.

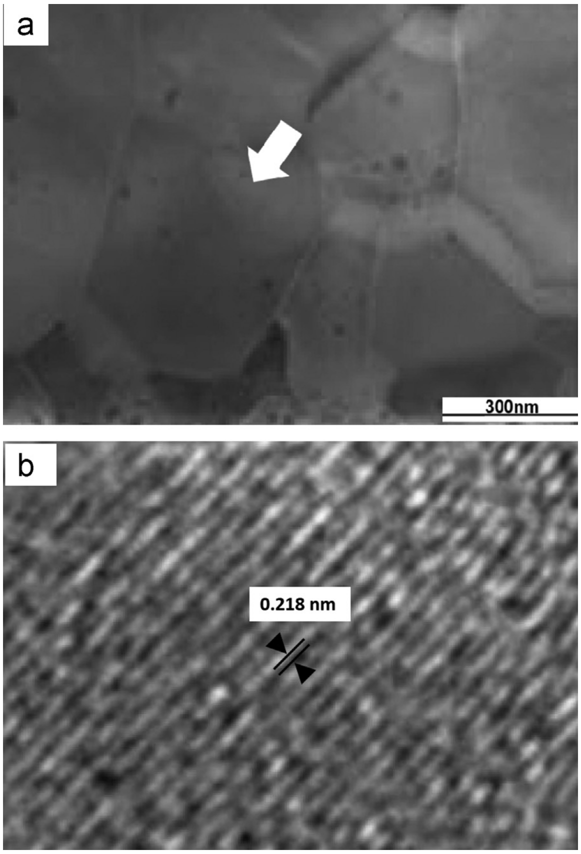

Fig. 11. TEM micrograph of the reaction layer of the AM−400 sample (a) and plane arrangement of the marked grain (b).

Detailed information about crystal structure of the bonding products are reported in Table 3. Reaction layer products showed face centered cubic (FCC) crystal structures with smaller unit cells than standard patterns near 0.20% for $MgAl_2O_4$ and 0.09% for $Mg_{0.388}Al_{2.4}1O_4$. Increasing bonding temperatures caused less unit cell contraction in AM-200 and AM-300 samples with $(Mg_{0.4}Al_{0.6})Al_{1.8}O_4$ phase from 1.04% to 0.11%. Same circumstance was measured for M-400 and AM-400 with $MgAl_2O_4$ structure. Increasing bonding temperature and mixing hydrides helped the formation of packed structures in the reaction layer. SEM micrograph and magnesium map of the hydride mixture nanopowders before and after heating and AM-400 sample reaction layer and magnesium concentration map are shown in Fig. 10. As seen, magnesium is mostly distributed along the alumina surface and formed mixed oxides (spinel) at the interface and slightly beneath the surface. The upper part of the micrograph (white) is attributed to alumina bodies. It is hard to find the reaction layer between alumina bodies. Darker parts of the micrograph are thought to be the reaction layer, where most of the Mg formed the spinel structure. TEM micrograph of the reaction layer in AM-400 sample is shown in Fig. 11. Packed grains with near 70 nm grain sizes were detected along the reaction layer. Lower part of the micrograph is attributed to alumina parts. Higher resolution of the grain in the middle of the reaction layer (marked in (a) micrograph) indicated presence arrays of parallel planes attributed to $MgAl_2O_4$ (200) plane with ~2.180 A *d* spacing.

3. Conclusions

Mixed hydride nanopowders were used for in-situ formation of oxide free metal/alloy nanopowders in the interlayer for diffusion bonding alumina ceramic parts. AlH_3, $Mg(AlH_4)_2$, and 1–1 M ratio mixtures decomposed to metallic and alloyed nanopowders during induction hot pressing. Free Al, Mg, and alloyed Mg(Al) nano particles were formed during decompositions. The interlayer materials reacted along alumina surfaces during bonding at 200, 300, and 400 °C. Formation of Al and Al–Mg mixed spinel oxides like $Mg_{0.388}Al_{2.41}O_4$, $(Mg_{0.4}Al_{0.6})Al_{1.8}O_4$, and $MgAl_2O_4$ improved shear strength of the joints. Diffusion bonded sample at 400 °C for 30 min under 20 MPa pressure showed shear strength of 202 MPa by forming spinel oxide with $MgAl_2O_4$ stoichiometry in the reaction layer. Presence of Mg along alumina surfaces and formation of nano-sized grains of spinel structure were detected via high resolution microscopy.

Acknowledgment

The authors would like to thank the Iranian Nanotechnology Society (I.N.S.) for their financial support on this study.

References

[1] H. Miyazaki, M. Hotta, H. Kita, Y. Izutsu, Joining of alumina with a porous alumina interlayer, Ceram. Int. 38 (2011) 1149–1155.

[2] R.J. Xie, M. Mitomo, G.D. Zhan, Diffusion bonding of silicon nitride using a superplastic b-SiAlON interlayer, J. Am. Ceram. Soc. 84 (2) (2001) 471–473.

[3] D. Travessa, M. Ferrante, G. den Ouden, Diffusion bonding of aluminum oxide to stainless steel using stress relief interlayers, J. Mater. Sci. Eng. A337 (2002) 287–296.

[4] L. Ceseracciu, E. Jimenez-Pique, T. Fett, M. Anglada, Contact strength of ceramic laminates, Compos. Sci. Techol. 68 (2008) 209–214.

[5] A. Li, C. Hua, M. Li, Y. Zhoua, Joining of Ti–Al–C ceramics by oxidation at low oxygen partial pressure, J. Eur. Ceram. Soc. 29 (2009) 2619–2625.

[6] M.G Nicholas, in: Joining of Ceramics, The University Press, Cambridge, UK, 1990.

[7] C.E. Scott, J.A. Brewer, Bend strengths for diffusion-bonded Al_2O_3, J. Am. Ceram. Soc. 69 (1986) 178–179.

[8] J.C. Feng, H.J. Liu, M. Naka, Reaction products growth kinetics during diffusion bonding of SiC ceramic to Ni–Cr alloy, Mat. Sci.Technol. 1 (2003) 137–142.

[9] Grant O. Cook III, Carl D. Sorensen, Overview of transient liquid phase and partial transient liquid phase bonding, J. Mater. Sci. 46 (2011) 5305–5323.

[10] M. Wei, D. Zhi, D.G. Brandon, Oxide ceramic laminates with highly textured a-alumina interlayers: I. texture control and laminate formation, J. Mater. Sci. 41 (2006) 7425–7436.

[11] S. Aravindan, R. Krishnamurthy, Joining of ceramic composites by microwave heating, Mater. Lett. 38 (1999) 245–249.

[12] J. Lemus-Ruiz, C. León-Patiño, R. Drew, Self-joining of Si_3N_4 using metal interlayers, Metall. Mater. Trans. 37A (2006) 69–76.

[13] Y. Zhai, T.H. North, Transient liquid-phase insert metal bonding of Al_2O_3 and AISI 304 stainless steel, J. Mater. Sci. 32 (1997) 1399–1404.

[14] H. Nishi, T. Araki, M. Eto, Diffusion bonding of alumina dispersion-strengthened copper ton 316 stainless steel with interlayer metals, Fusion Eng. Des. 39–40 (1998) 505–511.

[15] M. Eroglu, T.I. Khan, N. Orhan, Diffusion bonding between Ti–6A1–4V alloy and microduplex stainless steel, Mater. Sci. Technol. 18 (2002) 68–75.

[16] D.V. Dunford, P.G. Partridge, Transient liquid phase diffusion bonding of 8090 Al–Li alloy using copper interlayer, Mater. Sci. Technol. 14 (1998) 422–429.

[17] I.P. Jain, Pragya Jain, Ankur Jain, Review: novel hydrogen storage materials: a review of lightweight complex hydrides, J. Alloys Compd. 503 (2010) 303–339.

[18] J. Graetza, J.J. Reilly, V.A. Yartys, J.P. Maehlen, B.M. Bulychev, V.E. Antonov, B.P. Tarasov, I.E. Gabis, Review aluminum hydride as a hydrogen and energy storage material: past, present and future 5095 (2011) 5517–5528 (J. Alloys Compd.).

[19] N.C. Melvin, Joining of Materials, Hyde Park, NY, USA, 1991.

[20] I.E. Reimanis, Ceramic Joining, USA, The American Ceramic Society, Indiana, 1997.

[21] B. Hallstedt, Thermodynamic assessment of the system $MgO–Al_2O_3$, J. Am. Ceram. Soc. 75 (1992) 1497–1507.